Single-Crystal Germanium Growth on Amorphous Silicon

Kevin A. McComber, Xiaoman Duan, Jifeng Liu, Jurgen Michel, and Lionel C. Kimerling*

Growing single-crystal semiconductors directly on an amorphous substrate without epitaxy or wafer bonding has long been a significant fundamental challenge in materials science. Such technology is especially important for semiconductor devices that require cost-effective, high-throughput fabrication, including thin-film solar cells and transistors on glass substrates as well as large-scale active photonic circuits on Si using back-end-of-line CMOS technology. This work demonstrates a CMOS-compatible method of fabricating high-quality germanium single crystals on amorphous silicon at low temperatures of <450 °C. Grain orientation selection by geometric confinement of polycrystalline germanium films selectively grown on amorphous silicon by chemical vapor deposition is presented, where the confinement selects the fast-growing grains for extended growth and eventually leads to single crystalline material. Germanium crystals grown using this method exhibit (110) texture and twin-mediated growth. A model of confined growth is developed to predict the optimal confining channel dimensions for consistent, single-crystal growth. Germanium films grown from one-dimensional confinement exhibit a 200% grain size increase at 1 μm film thickness compared to unconfined films, while 2D confinement growth achieved single crystal Ge. The area of single crystalline Ge on amorphous layers is only limited by the growth time. Significant enhancement in room temperature photoluminescence and reduction in residual carrier density have been achieved using confined growth, demonstrating excellent optoelectronic properties. This growth method is readily extensible to any materials system capable of selective non-epitaxial deposition, thus allowing for the fabrication of devices from high-quality single crystal material when only an amorphous substrate is available.

1. Introduction

1.1. Background

The production of high-quality crystalline material on an amorphous substrate using low processing temperatures is extremely challenging. For decades, researchers have attempted to fabricate large-grained polycrystalline semiconductor materials on amorphous templates while keeping processing temperatures low, using techniques such as laser annealing,[1–3] graphoepitaxy,[4,5] metal-induced crystallization,[6–10] or some combination thereof.[11] Increasing a polycrystalline material's grain size decreases its grain boundary (defect) density and subsequently mitigates such device-degrading issues as dark current, unwanted free carriers, and carrier scattering. A large amount of work has focused on attempting to increase the grain size of polycrystalline germanium (poly-Ge), as Ge has desirable optical and electrical properties. However, all previously-employed methods of increasing poly-Ge's grain size have suffered from serious drawbacks, such as low throughput and incompatibilities with complementary metal-oxide-semiconductor (CMOS) processing.

Here, we present a method that employs the selective growth of germanium on amorphous silicon by ultra-high vacuum chemical vapor deposition (UHVCVD) at low temperatures (T < 450 °C). Selective growth by UHVCVD gives control over the precise locations of germanium growth, and growth confinement promotes the selection of fast-growing germanium grains. These fast-growing grains serve as the seeds for further single-crystalline germanium growth. This high-throughput, CMOS-compatible method for the monolithic fabrication of germanium single crystals on amorphous silicon facilitates the fabrication of germanium devices in applications requiring low processing temperatures and lacking single-crystal substrates, such as back-end-of-line photonic device manufacturing.

1.2. Theory

When a polycrystalline material is deposited on a surface, nuclei with random crystallographic orientations form and subsequently grow into crystalline grains upon continued material deposition. A grain's particular crystallographic plane parallel to the substrate surface defines that grain's orientation (e.g., if a grain has its (110) plane parallel to the substrate, it has a (110) orientation).

Each grain's orientation determines the rate at which the grain grows during deposition. This orientation-dependent

Dr. K. A. McComber, Dr. X. Duan, Prof. J. Liu, Dr. J. Michel, Prof. L. C. Kimerling
Massachusetts Institute of Technology
77 Massachusetts Avenue, Room 13-4110
Cambridge, MA 02139, USA
E-mail: jmichel@mit.edu
Prof. J. Liu
Thayer School of Engineering
Dartmouth College
8000 Cummings Hall, Rm. C227, Hanover, NH 03755, USA

DOI: 10.1002/adfm.201102015

grain growth rate is the grain growth velocity anisotropy, and its basis lies in the underlying crystal unit cell. Depending on the crystal structure, certain crystal planes will possess higher or lower surface free energies with respect to the other planes in the lattice. The plane with the lowest surface free energy will tend to grow very slowly in its normal direction, as there are few sites on the plane for atom adsorption. Conversely, the plane with the highest surface free energy will tend to grow quickly in its normal direction. The grains with the fast-growing plane's normal oriented in the direction of the growth (i.e. with the fast-growing plane parallel to the substrate) will eventually overgrow the surrounding slower-growing grains and dominate the nature of the film. When the film no longer has a random distribution of grain orientations, it is said to have a certain texture (such that, for example, a film with predominantly (110)-oriented grains would be said to have a (110) texture).

Our work concerns the deposition of polycrystalline germanium (Ge), so we will concentrate on Ge and its diamond cubic lattice. In the case of Ge, the {111} planes are of principal importance because they have the highest planar atomic packing density, and thus the lowest surface free energy.[12] The {111} planes therefore often form the boundaries of a growing crystal, and two grain orientations are theoretically possible within the confines of the {111} surface boundaries – these are growth with a <100> orientation and growth with a <110> orientation.[13] The <100> directions span between two tips of the octahedron bounded by {111} facets, and the <110> lie along the edges of the octahedron. Assuming equal normal growth velocities of the {111} bounding planes, the <100> directions should grow faster than the <110> because the enhanced growth rate seen at the octahedron's tips from normal {111} growth is greater than that seen at its edges. This purely geometrical argument, however, does not always produce the correct result: diamond films bounded by {111} facets have been grown with a (110) texture.

The concept needed to correct this apparent incongruence is that of twinning. The energy required to create a twin in Ge (as well as Si and diamond) is nearly zero,[14] and such crystals tend to twin easily on {111}, where the post-twin lattice grows at an angle of 60° to the pre-twin lattice. Thus, if a grain is growing with <100> orientation and twins, its orientation will no longer be <100>, as the <100> only form 90° angles with each other. However, if a grain is growing with <110> orientation and twins, it can still grow in a <110> orientation as some of the <110> form 60° angles with each other. Thus, twinned <100> orientations will no longer be favored for growth, but some twinned <110> orientations may continue to grow after twinning.

The {111} planes that bound each polycrystalline Ge grain have very slow normal growth and will thus cause the grain growth to stagnate as their slow normal growth impedes the growth of the crystal. However, as a twin in Ge requires very little energy, the material may form a series of twins that enhance the growth rate with negligible energetic penalty.[15] The twins intersect the crystal surface, and the line of intersection provides heterogeneous surface nucleation sites on the Ge crystal at which another layer may start to form; multiple twins are required for long-range growth, as the growth on one twin eventually self-terminates. In the case of <110> Ge crystals grown from the melt, the crystal growth is the result of simultaneous growth in two <211> directions, mediated by layer nucleation at twin boundaries intersecting the crystal surface.[16,17] As growth from the melt and growth from the vapor phase both require crystal surface layer nucleation to continue the crystal growth, this twin-mediated growth phenomenon is expected to hold true for vapor-phase Ge crystal deposition as well.

Despite the large body of knowledge regarding polycrystalline germanium growth, the ability to obtain high-quality, single-crystal germanium from growth on an amorphous substrate has eluded researchers for decades. The most frequently attempted method of single-crystal germanium formation on amorphous substrates, metal-induced lateral crystallization (MILC), has been shown to produce enhanced grain sizes over as-deposited samples, but suffers from a high metal content in the final material that can be detrimental to device operation. The metals used in MILC are often not compatible with complementary metal-oxide-semiconductor (CMOS) processes, so they cannot enter a CMOS fabrication facility. The MILC process also has low throughput. Other techniques, such as laser annealing and graphoepitaxy, also suffer from setbacks in throughput and/or cost and cannot be implemented in manufacturing.

The method presented here overcomes these challenges and allows for the high-throughput, CMOS-compatible production of single-crystal Ge on amorphous silicon (a-Si) at low temperatures. We employ selective Ge deposition, in which Ge deposits on Si and not on SiO_2, to define specific locations in which the Ge nucleates on a-Si. By subsequently growing the polycrystalline Ge film in confined regions, we are able to utilize the film's grain growth velocity anisotropy to select the fast-growing grains. These grains serve as the seeds for further single-crystal Ge growth at well-defined sites.

2. Results and Discussion

2.1. Crystallography

The two types of growth confinement structures employed in this work are illustrated in **Figure 1**a,b, where Ge selectively grows from areas of exposed a-Si. Figure 1a shows 1D (vertical) confinement of the Ge growth, where the Ge can only grow laterally while it is under the top oxide. Figure 1b depicts 2D (vertical and lateral) confinement of the growth, where the Ge can only grow from left to right within the oxide-enclosed region. In both the case illustrated in Figure 1a and that in Figure 1b, the confined area in which the Ge grows will be called the channel. In 1D confinement, as shown in Figure 1a, the channel's length and height are given by d and h, respectively, such that the ratio $\frac{d}{h}$ is the channel's aspect ratio. In 2D confinement, as depicted in Figure 1b, the channel's length and height are defined as in 1D confinement, but the dimension w is added to define the channel's width. The aspect ratio for 2D confinement is $\frac{d}{\sqrt{hw}}$.

Figure 2a shows a perspective schematic and a plan-view scanning electron microscope (SEM) image of a Ge growth emerging from a 1D confinement structure, like that in Figure 1a, with aspect ratio ~2.5. The Ge nucleates selectively on the a-Si and grows in the plane of the wafer, eventually

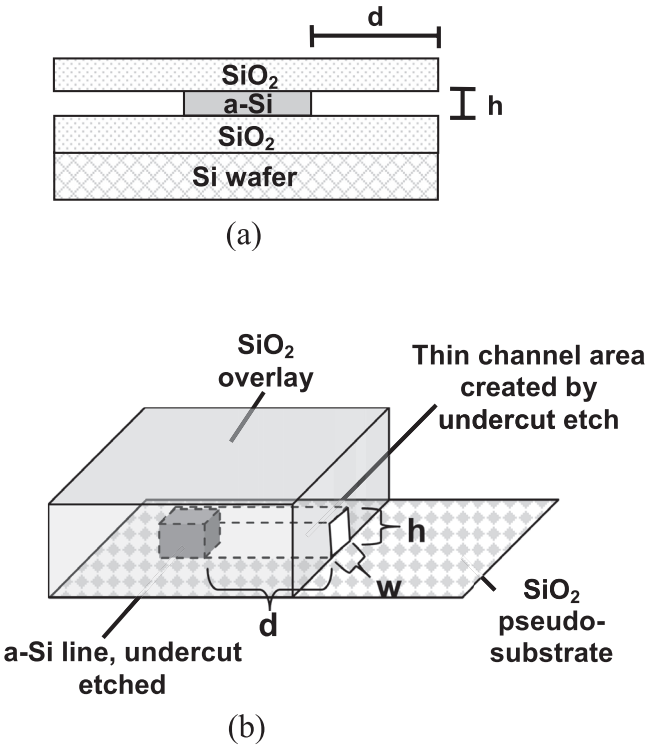

Figure 1. a) Cross-section schematic of the structure for 1D-confined Ge growth, where *d* is the channel length and *h* is the channel height. b) Schematic of the structure for 2D-confined Ge growth, with *d* and *h* as in (a) and *w* as the channel width. Dimensions are not to scale.

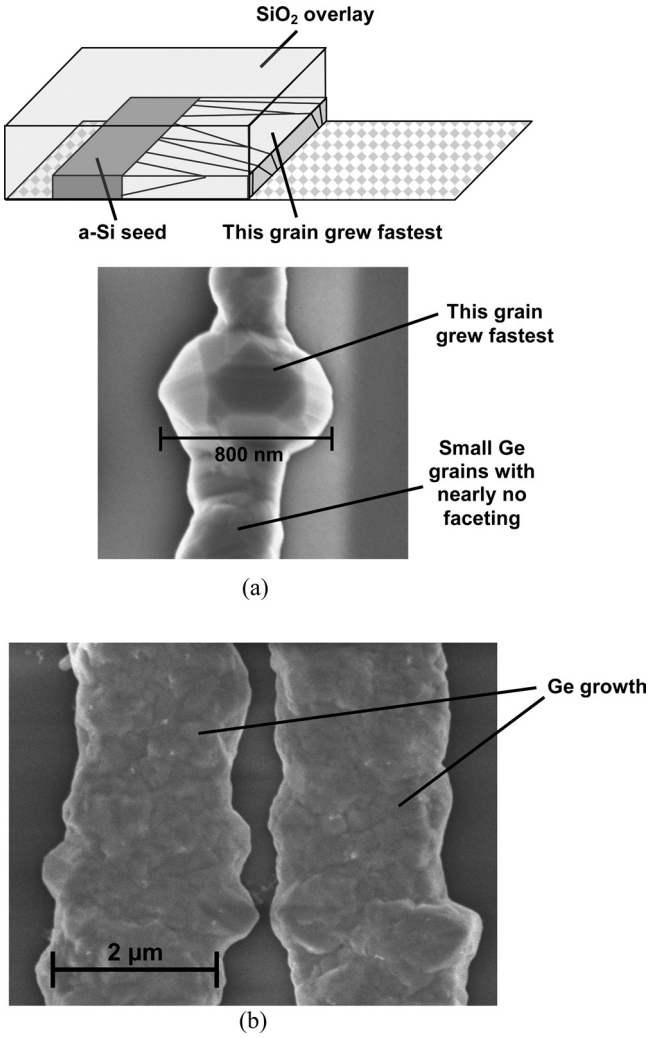

Figure 2. a) A schematic of 1D-confined growth (not to scale), showing poly-Ge grain boundaries and one dominating, fast-growing grain (growth outside the channel removed for ease of viewing), and a plan-view image of 1D-confined Ge growth from a-Si (aspect ratio ~2.5), showing a large, dominating grain with obvious faceting developing among smaller grains. The Ge shown is that which emerges from the channel. b) Plan-view image of barely-confined Ge (aspect ratio ~0.25). Faceting in (b) is not readily apparent, as it is in (a).

emerging from under the PECVD oxide; this type of growth will be called 1D geometrically-confined lateral growth (1D GCLG).

In the growth depicted in Figure 2a, the confinement in the vertical dimension serves to select some grains, but the lateral dimension (in the plane of the substrate wafer) is still unconfined. In some areas of the growth in Figure 2a, the fast-growing grain is not selected before growing out of the channel. However, in one area, a fast-growing grain was able to overtake its neighboring grains and dominate the growth. As the dominant grain is the fast-growing grain, it stands to reason that it produces the region with the most extensive growth (the largest bulge) in the SEM image of Figure 2a. Figure 2b shows a microscopy image of selectively-grown poly-Ge with very little confinement (aspect ratio ~0.25) for comparison to Figure 2a; no faceting is obvious in Figure 2b. This comparison shows that confinement of the Ge during growth promotes the evolution of large Ge grains.

Figure 3a shows a cross-section SEM image of GCLG Ge from a 1D confinement structure, giving a clear view of the structure, growth, and growth facets. Figure 3b is a cross-section transmission electron microscope (TEM) image of a 1D-confined growth, in which a multitude of defects near the a-Si seed are visible as variations in the image's contrast, showing that the top and bottom oxide walls serve as points for defect termination. Selected area diffraction in the TEM confirms that the Ge near the a-Si seed is highly polycrystalline, while Ge at the open end of the channel is monocrystalline. TEM and electron backscatter diffraction (EBSD) show that the grain size in a film grown from 1D confinement (aspect ratio 4.5) at 1 μm thickness is approximately three times that in unconfined films at the same thickness.

Figure 4 shows a plan-view SEM image of Ge grown from a patterned a-Si seed layer for 2D-confined growth. The a-Si layer was patterned into very narrow and thin lines (<500 nm in width, <100 nm in height) followed by selective etching so that the growth channels were also correspondingly narrow; in this case, growth was confined in both the vertical dimension and one lateral dimension, and will be referred to as 2D geometrically-confined lateral growth (2D GCLG). The 2D GCLG structure additionally allows us to specify the precise locations of large crystal growths on the sample, which is a requirement for the successful fabrication of devices from this material.

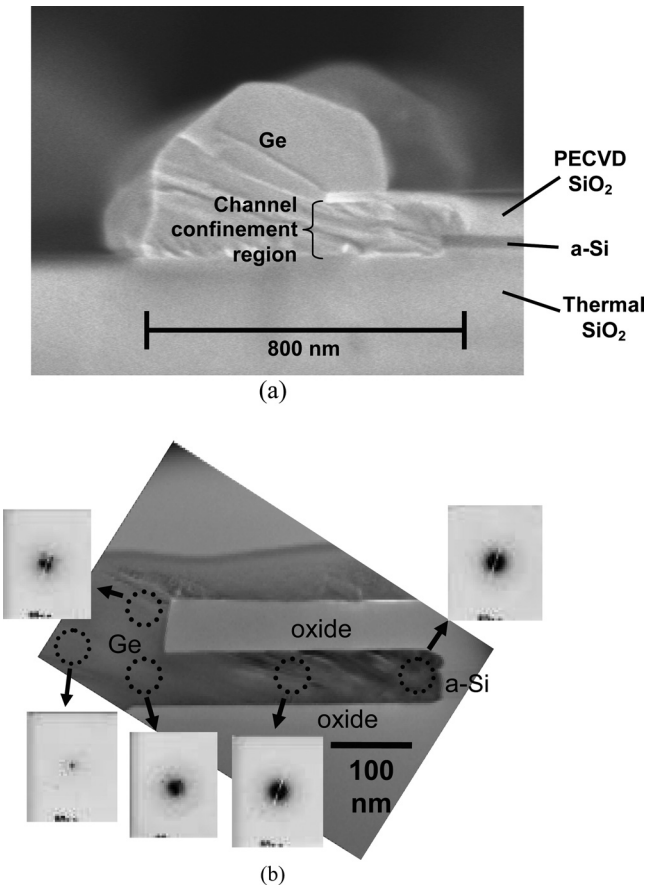

Figure 3. a) Cross-section SEM image of 1D GCLG from a-Si. Faceting is visible in the Ge. The PECVD oxide has been partially etched by the wet chemical cleaning process used to prepare the sample, widening the channel confinement region from the as-fabricated state. b) Cross-section TEM microscopy image (bright field, 200 kV) of the 1D GCLG structure and Ge growth. The PECVD oxide etching issue in this sample has been minimized.

In both Figures 2a and 4, it is evident that a region of the growth front (in the case of Figure 4, the entire growth front) has a faceted nature (i.e. is covered by multiple planar surfaces), across areas on the order of a micrometer in size. These

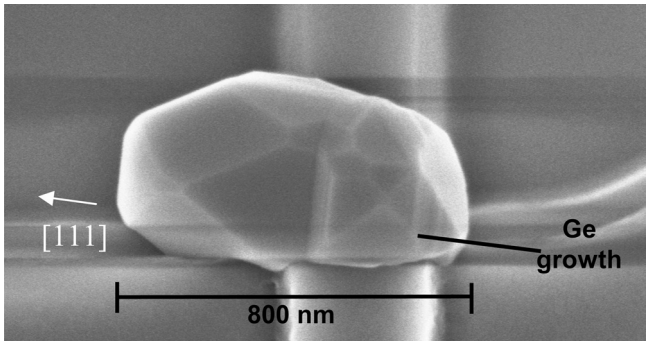

Figure 4. Plan-view SEM image of Ge 2D GCLG. Note the faceting of the growth, indicating grain size on the order of the size of the growth. The channel is the bright white column in the bottom of the image. The {111} twin normal direction is indicated.

faceted regions are large crystals induced by the constraint of the material's growth. As-deposited grains of poly-Ge on a-Si at these growth temperatures and times would be on the order of 100 nm in size, so the confined growths show approximately an order of magnitude increase in grain size, and the size is limited only by the duration of the growth.

However, it is also evident from the crystal in Figure 4 that the faceting is interrupted by what appear to be line defects on the surface. Using EBSD, the presence of Σ3 (twin) and, in a few cases, Σ9 boundaries has been confirmed in the large Ge crystals grown from 2D confinement, but no other coincidence site lattice boundaries are evident. As both Σ3 and Σ9 boundaries are coherent boundaries and thus have no dangling bonds that could cause mid-gap energy states,[14,18,19] we expect no adverse effects on devices made from material containing these boundaries. In Figure 4, the twin boundary visible in the image occurs on one of the {111} planes; the [111] normal direction is indicated in the figure. Our observation of twins in our large crystals matches with the prediction that our confined growths would have to contain twins for long-range growth at a reasonable rate.

As previously mentioned, twinning in FCC polycrystalline materials causes (110) texturing; however, untwinned films may also grow with a (110) texture if they can sustain both (111) and (100) facets.[20] X-ray diffraction studies of our blanket poly-Ge (unconfined) films confirm that our poly-Ge has a (110) texture, but EBSD studies of our Ge show that the facets are {111} and that twins are present in both confined and unconfined growths. Thus, the (110) texture of our poly-Ge is caused by twinning. EBSD studies of our confined growths show that the 2D GCLG material is also (110)-oriented in the channels, as would be expected due to twinning in the confined Ge.

The present work also extends previous research performed on twin-mediated crystal growth. Ge crystals with <110> orientation grow from the melt by the adsorption of Ge adatoms at the intersections of twin boundaries with the Ge surface.[16,17] As in the case of the Ge <110>-oriented crystals grown from the melt, we observed {111} planes bounding our crystals as well as twins on the {111} planes. We have also observed striking similarities to the ideal <110>-oriented crystal morphology, shown in **Figure 5**a; in Figure 5b is shown a Ge crystal grown during our work with 2D GCLG, using a 6-hour growth at 450 °C and a subsequent 2.5-hour growth at 650 °C to accelerate the growth process. We also performed growths with obstacles between the a-Si seed layer and the channel exit in order to block line-of-sight twin propagation and we still observed twins in every emerging growth; we thus confirm that twinning is strongly preferred for growth, and that the twins may form during growth. We assert that the theory developed for Ge crystals grown from the melt at low undercooling holds for Ge crystals deposited from the vapor phase on a-Si by UHVCVD, and that our crystals grow primarily by twin-mediated surface atom adsorption.

2.2. Channel Design

Knowing the ideal channel geometry needed to obtain the best possible material would allow for the design of an optimal channel. We define the best possible growth outcome as one

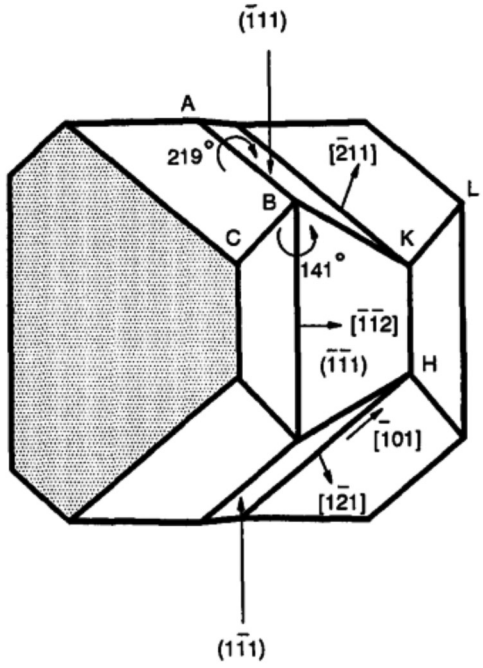

(a)

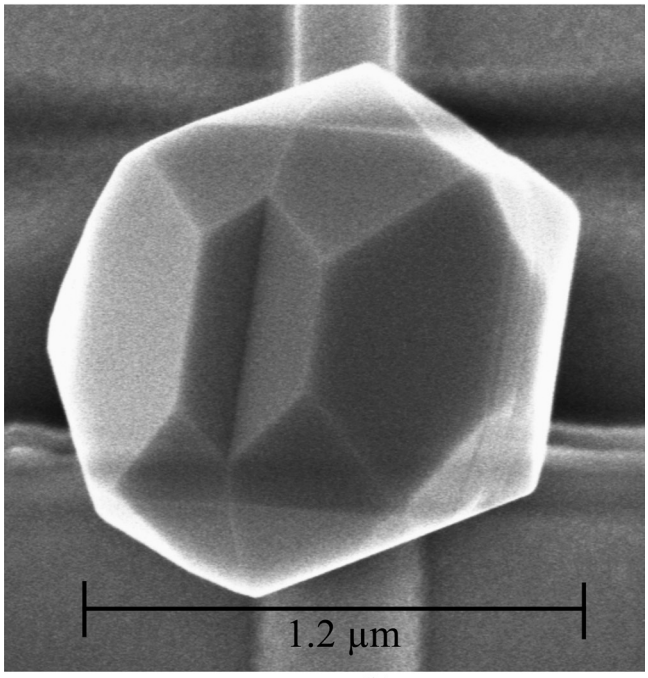

(b)

Figure 5. a) Idealized schematic from Ref. 17, showing the planes and facets associated with a <110> Ge crystal. b) Ge crystal grown in the current work from 2D confinement. Reproduced with permission.[17] Copyright 1994, Elsevier.

in which growths emerge from every channel, are of uniform size, are as large as possible, and contain as few grains as possible (i.e., are most monocrystalline); the optimum channel geometry would lead to such a growth. In order to understand the effects of the channel geometry on the confined Ge growth, the channel was modeled as a rectangular prism, with dimensions d, h, and w, as shown in Figure 1b. The ratio Ω_c/Ω_h was calculated, where Ω_c is the solid angle of the channel's opening as seen from the center of the a-Si nucleation seed, and Ω_n is the solid angle of the four standard stereographic triangles surrounding a single (110) pole; outside the area defined by Ω_n, the crystallographic symmetry dictates that another of the {110} would be closer to the a-Si normal, so Ω_n defines the area swept out by the possible misorientations of one (110) pole with respect to the a-Si normal. The values of Ω_c and Ω_n are given by Equations (1) and (2):

$$\Omega_c = 4 \arcsin \frac{hw}{\sqrt{(4d^2 + w^2)(4d^2 + h^2)}} \quad (1)$$

and

$$\Omega_n = 2\pi * \frac{4}{24} = \frac{\pi}{3} \quad (2)$$

This ratio was multiplied by the approximate number of nuclei on the channel's a-Si seed, equal to the area of the seed in the channel (hw) divided by the average area of a Ge grain, A_G, on a-Si at 450 °C (approximately 500 nm^2 from our TEM observations), to give the average total number of grains expected to emerge from a channel. This model assumes that poly-Ge nuclei orientations are random, which, based on x-ray diffraction data from very thin poly-Ge films deposited in our system, is nearly correct. The model also assumes that, if a grain does not have one of its <110> oriented such that it will intersect the area defined by the channel exit, it will self-terminate and not emerge from the channel in the time of the growth. Images of growths that have self-terminated in the channels support this assumption. The model further assumes there are no transport issues for the GeH_4 gas to reach the a-Si seed, which is correct, based on our experimental observations and the fact that the Knudsen number for such a system is extremely high in the channels (~10^6), so flow in the channels must be molecular. Finally, the model assumes the a-Si seed area is much larger than the size of the Ge grain on the seed, such that a multitude of grains may exist and so that probability may be employed. The total number of grains, N_G, expected to emerge from a channel of height h, width w, and length d, is given by Equation (3):

$$N_G = \frac{\Omega_c}{\Omega_h} * \frac{hw}{A_G} \quad (3)$$

Setting $N_G = 1$ defines the channel's geometry at which there is a cutoff point: for geometries giving $N_G < 1$, growth is not expected to consistently emerge from the channel, while for $N_G \geq 1$, growths are expected from every channel. **Figure 6** shows experimental data for growth emergence vs. N_G, taken from numerous channel arrays with at least 50 channels per array. The fabricated channels have heights between 35 nm and 120 nm, widths between 145 nm and 600 nm, and lengths between 450 nm and 1250 nm; the blanket growth from the same experiment had thickness ~1650 nm, so the growth was of sufficient duration to potentially emerge from the channels. It can be seen that the model predicts nearly the correct relation

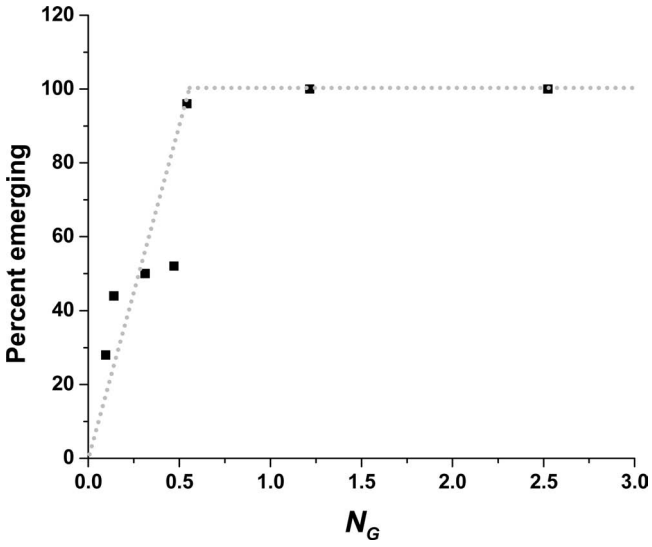

Figure 6. Percent of growths that emerge from their channels vs. N_G, with $A_G = 500$ nm^2. 100% of growths emerge for values of N_G higher than those shown here. The dotted lines are added to guide the eye.

between emergence and N_G, as growths with N_G greater than approximately 0.6 show consistent emergence. This discrepancy is easily understood, as the model conservatively assumes that *any* growing grain that does not have a {110} normal that will intersect the area defined by the channel exit will self-terminate, though we know that grains can also grow (albeit more slowly) in non-{110}-normal directions. Thus, we would expect to see growth emergence for even lower values of N_G than predicted, as is indeed the case. Despite the discrepancy, the value of N_G still has strong physical significance and is of paramount importance when determining the ideal channel geometry, as will be seen.

The relation between growth extent and N_G as well as between growth extent variation and N_G is depicted in **Figure 7**a and b, respectively. The growth extent is given as a length and is found by measuring at least 20 growths' dimensions in the direction of their channels and taking the average, and the growth extent variation is calculated as the coefficient of variation (CV) of the growth extent. All channels investigated for the generation of the plots had lengths in the range of 500 nm to 700 nm so as to minimize the effect of the channel length on the resulting growth extent. As seen in Figure 7a, the growth extent initially increases with N_G as more fast-growing grains are correctly oriented to emerge from the channel and are also strongly confined. The growth extent then attains a maximum in the range $2.0 \leq N_G \leq 3.0$ and subsequently decreases as the confinement is further reduced (N_G is increased) and the fast-growing grains are no longer efficiently selected. In Figure 7b, the growths' CVs are constant at approximately 0.3, though a minimum is observed in the range $2.0 \leq N_G \leq 3.0$. Based on the experimental data, the optimal N_G, chosen to maximize growth emergence frequency, growth uniformity, and growth size, lies in the range $2.0 \leq N_G \leq 3.0$. However, in order to ensure that the fewest (110)-oriented grains emerge from any given channel while still maintaining consistent emergence

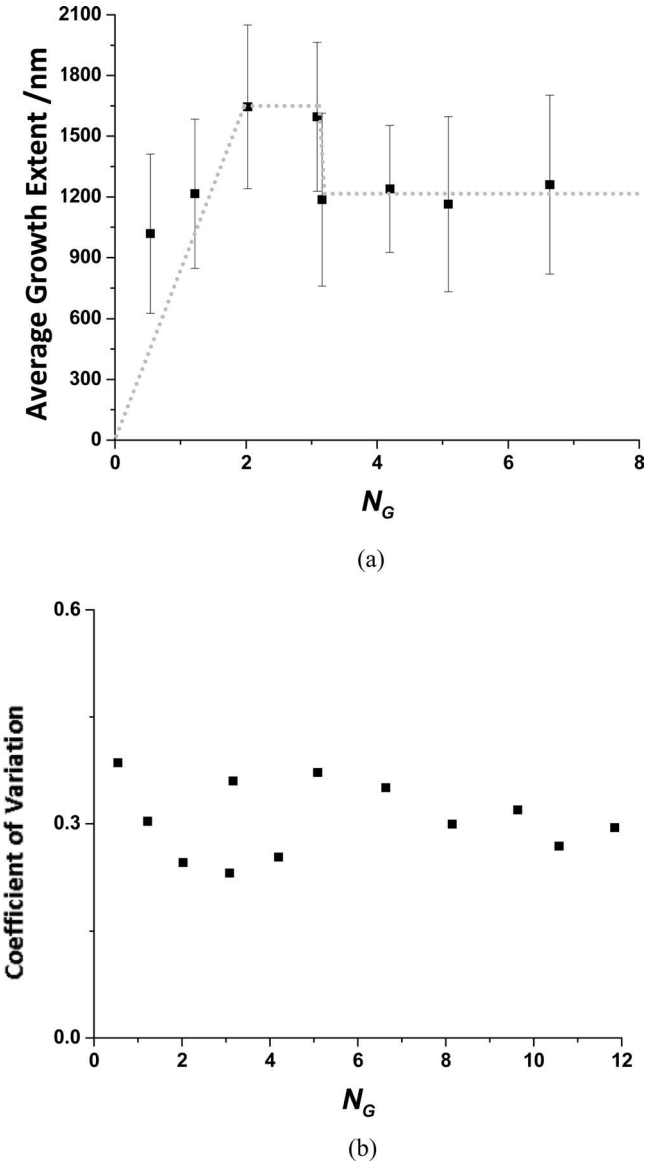

Figure 7. a) Growth extent vs. N_G, and b) growth extent coefficient of variation vs. N_G, both with $A_G = 500$ nm^2. Dotted lines are added to guide the eye, and the error bars in (a) are ± one standard deviation.

across many channels, a value of N_G in the lower part of this range (i.e. nearest 2.0) should be chosen. This finding sets restrictions on the relations among the length, width, and height of a channel to obtain the best material quality (emergence, uniformity, extent, and monocrystallinity) from the confined growths.

This single constraint is not enough to satisfactorily define the optimum channel geometry, however; for example, an extremely wide but very thin channel with a suitable length could have $N_G = 2.0$, though it is obvious that this case is not ideal because a fast-growing grain could not overcome all other grains in a very wide (albeit thin) channel. Thus, the channel width and height should be chosen to be as equal in size as possible in order to maximize the symmetry of the channel and

thus minimize the distance any grains need to grow in order to overtake all other grains in the channel. Furthermore, the geometry of the channel should also be chosen to obtain the shortest channel length, within the above framework, in order to minimize the growth time needed for growth emergence from the channels. Thus, we define three ideal properties of a 2D confinement channel:

(1) $N_G = 2.0$
(2) Channel height = channel width ($h = w$)
(3) Channel length (d) as short as possible, subject to satisfaction of (1)

2.3. Optoelectronic properties

One potential application for the single crystals deposited by this method is the back-end-of-line fabrication of photonic devices for use in electronic-photonic 3D-integrated circuits. For the successful fabrication of high-performance active p-i-n photonic devices, an intrinsic (undoped) region with low carrier density (~10^{16} cm^{-3}) is necessary. As-deposited, unconfined poly-Ge growth shows a strong p-type character (p~10^{18} cm^{-3}) that is attributed to the presence of acceptor states in defects.[21–26] **Figure 8** presents data from Hall effect measurements on a number of samples, showing hole concentration versus thickness for three unconfined poly-Ge films as well as three films grown from 1D confinement structures. It is evident that thicker unconfined growths have a lower hole density compared to thinner unconfined growths, congruent with the concept of an increasing grain size with increasing film thickness and thus a decreasing carrier density due to a decreasing grain boundary density. The data also show that the films grown from 1D confinement have lower defect densities than all unconfined films measured,

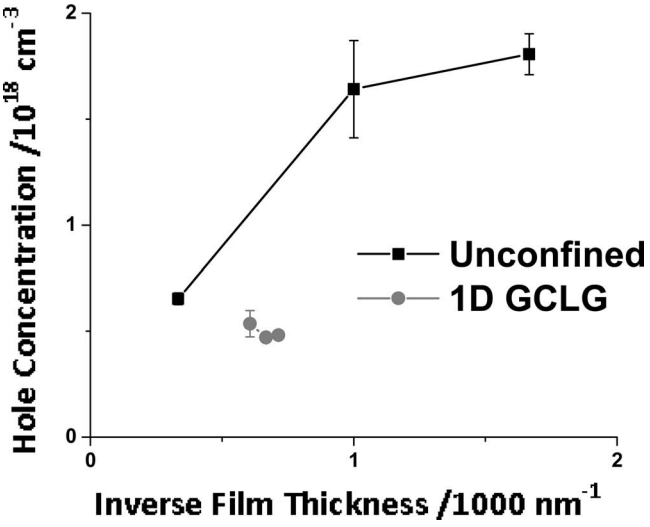

Figure 8. Hole concentration versus inverse film thickness for three unconfined poly-Ge films as well as three films grown from 1D confinement. Lines are added to guide the eye and error bars are ± one standard deviation.

indicating that the confinement structure reduces the film defect density from that of an unconfined film. Additionally, Hall effect measurements show an increased hole mobility in films grown from 1D confinement compared to blanket films of similar thickness; this result is also congruent with the concept of growth confinement lowering the Ge defect density, since defects cause carrier scattering and thus lower the mobility. Hall effect measurements were not performed on material grown from 2D confinement due to difficulties in contacting such small crystals.

We can attempt to calculate the expected number of carriers in a blanket poly-Ge film in order to quantitatively compare our films' electrical properties to that expected from a film with defect-caused p-type character. We consider only the grain boundaries to cause p-type defects here, as the boundaries will likely dominate the film's defect population. We can use a close-packed array of hexagonal prisms with the long axes through the film's thickness to model the grains in the films. From TEM images we know that the average grain size in an as-deposited poly-Ge film of 1 μm thickness is on the order of 100 nm. If we define the grain's size as the distance between two parallel edges of a hexagon in the array, this gives the length of each of the hexagon's sides (L) as 57 nm, such that the area of each hexagon (grain) is 8660 nm^2. Thus, in one cm^2 of 1-μm-thick film, there are 1.15×10^{10} grains, each with 1.71×10^{-9} cm^2 grain boundary area ($3L \times 1$ μm), for a total grain boundary area of 19.7 cm^2. We can approximate there to be ~10^{13} cm^{-2} carrier density in the grain boundaries.[27] Thus, in our 10^{-4} cm^3 of film, we expect to see 1.97×10^{14} carriers (19.7 cm^2 × 10^{13} carriers/cm^2), or 1.97×10^{18} cm^{-3} carrier density. This is close to our observed carrier density of ~1.6×10^{18} cm^{-3} for a 1-um-thick as-deposited film.

Photoluminescence measurements on unconfined films as well as growths from 1D confinement and 2D confinement were performed, and the results are presented in **Figure 9**. The data in Figure 9a are normalized for film volume. In Figure 9b, while the unconfined material formed a continuous film, the materials grown from 1D and 2D confinement did not, so the data could not be normalized to film volume. However, such normalization would only serve to extend the difference between the unconfined and confined materials. The amount of material under observation between the 1D and 2D confinement samples was, by inspection, approximately equal. However, the laser spot used in the PL measurement is large relative to the confining structure and penetrates the top oxide, so the poor material in the 1D GCLG channel is also probed, likely giving lower PL than if only the material outside the channel were investigated. These results demonstrate that the defect density in material grown from confinement is reduced as the degree of confinement is increased.

3. Conclusions

This work advances decades of research in numerous fields by demonstrating the possibility of single-crystal material growth from an amorphous substrate. By depositing Ge selectively on a-Si and growing it through confining channels, we obtain single-crystal Ge in well-defined locations. Growth confinement

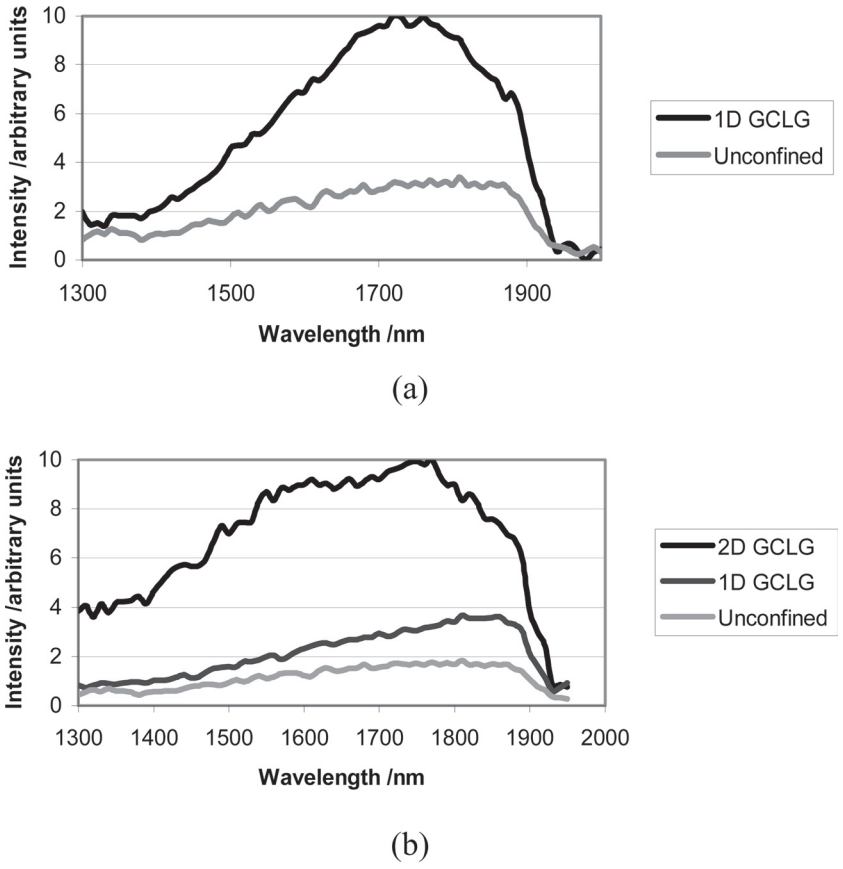

Figure 9. Photoluminescence spectra from a) an unconfined film and a film grown from 1D confinement, normalized to film volume, and b) an unconfined film and material grown from 1D and 2D confinement, not normalized to material volume. In (a), the 1D GCLG structure had an aspect ratio of 4.5; in (b), the 1D GCLG structure had an aspect ratio of 6.7 and the 2D GCLG sample had $N_G = 3.2$.

selects the fast-growing grains, which serve as the seeds for single-crystal growth outside the confining region. The single crystals grow with (110) orientations and their growth is mediated by the formation of twins that both help select the (110) orientation and enhance the crystals' growth rates in that direction. We developed a model to predict the optimal channel geometries for single-crystal growth so that other researchers may effectively utilize this method. The material grown from confinement was shown to have a lower defect density than as-deposited blanket poly-Ge, signaling its improved applicability to device fabrication.

The low-T and CMOS-compatible nature of the single-crystal Ge deposition means this material is promising for the fabrication of back-end-of-line photonic devices, thin film transistors on cheap glass substrates, pseudosubstrates for III-V-on-Ge heteroepitaxial deposition, and a host of other potential applications. Furthermore, the deposition of single-crystal material on an amorphous substrate by confined growth is readily extensible to any materials system capable of selective non-epitaxial deposition, thus allowing for the fabrication of devices from high-quality material when only an amorphous substrate is available.

4. Experimental Section

Sample fabrication began with the growth of 500 nm of thermal SiO_2 on 150 mm p-type (100) Si wafers. Although this step does not conform to the low thermal budget of the process, it is accepted that low-T-deposited SiO_2 (such as that deposited by plasma-enhanced chemical vapor deposition at 400 °C) may be easily substituted with no effect on the experimental results; thermally-grown SiO_2 was used solely to provide an oxide pseudosubstrate. Amorphous silicon of 40 to 120 nm thickness was then deposited by plasma-enhanced chemical vapor deposition (PECVD) at 350 °C on the thermal SiO_2 and, in some cases, patterned using photolithography. This was followed by a deposition of 200–300 nm of PECVD SiO_2 (oxide) on the a-Si at 400 °C. This PECVD oxide was patterned by photolithography and reactive ion etching to expose the underlying a-Si. The a-Si was then reactive ion etched and subsequently undercut etched beneath the top oxide using a tetramethylammonium hydroxide selective wet etch.

Samples were cleaned using piranha solution and the RCA method, and loaded into a hot-walled UHVCVD chamber idling at 450 °C and $<10^{-8}$ Torr. The samples were annealed for up to 2 hours at 450 °C to degas hydrogen from the PECVD a-Si and oxide. GeH_4 was subsequently flowed at 7.5 sccm for 4 to 16 hours at 450 °C for selective Ge deposition on the a-Si; the partial pressure of GeH_4 was 3×10^{-4} Torr in all experiments. The samples were then removed from the growth chamber and allowed to cool to room temperature before being removed from vacuum.

While the HF bath portion of the RCA clean did etch the SiO_2 deposited by PECVD, this etching was easily controlled by limiting the time the wafers spent in HF and should not be a limitation to the viability of this process in a low-T fabrication environment.

Acknowledgements

The authors would like to thank the National Science Foundation and the Defense Advanced Research Projects Agency for support, as well as the MIT Microsystems Technology Laboratories and the MIT Center for Materials Science and Engineering for their assistance and the use of their facilities. The authors are also grateful to Carl Thompson and Christopher Schuh for insightful discussions.

Received: August 24, 2011
Revised: November 3, 2011
Published online: December 21, 2011

[1] S. Caune, J. Marfaing, W. Marine, *Appl. Surf. Sci.* **1989**, *36*, 597.
[2] H. J. Kim, J. S. Im, *Appl. Phys. Lett.* **1996**, *68*, 1513.
[3] B. L Sopori, L. W. Chen, J. Alleman, R. Matson, N. M. Ravindra, T. Y. Tan, *Mat. Res. Soc. Symp. Proc.* **1998**, *485*, 95.
[4] T. Yonehara, H. I. Smith, C. V. Thompson, J. E. Palmer, *Appl. Phys. Lett.* **1984**, *45*, 631.
[5] H. I. Smith, C. V. Thompson, H. A. Atwater, *J. Cryst. Growth* **1983**, *65*, 337.

[6] H. Kanno, K. Atsushi, T. Sadoh, M. Miyao, *Mat. Sci. Semicond. Process.* **2005**, *8*, 83.
[7] C. H. Yu, P. H. Yeh, S. L. Cheng, L. J. Chen, L. W. Cheng, *Thin Solid Films*, **2004**, *356*, 469–470.
[8] C. M. Yang, H. A. Atwater, *Appl. Phys. Lett.* **1996**, *68*, 3392.
[9] H. Tanabe, C. M. Chen, H. A. Atwater, *Appl. Phys. Lett.* **2000**, *77*, 4325.
[10] L. R. Munix, C. T. M. Ribeiro, A. R. Zanatta, I. Chambouleyron, *J. Phys.: Condens. Matter* **2007**, *19*, 076206 1.
[11] H. I. Smith, C. V. Thompson, M. W. Geis, R. A. Lemons, M. A. Bosch, *J. Electrochem. Soc.* **1983**, *130*, 2050.
[12] Z. Gai, W. S. Yang, R. G. Zhao, T. Sakurai, *Phys. Rev. B: Condens. Matter Mater. Phys.* **1999**, *59*, 15230.
[13] C. Wild, N. Herres, P. Koidl, *J. Appl. Phys.* **1990**, *68*, 973.
[14] J. Narayan, A. S. Nandedkar, *Philos. Mag. B* **1991**, *63*, 1181.
[15] R. S. Wagner, *Acta Metall.* **1960**, *8*, 57.
[16] C. F. Lau, H. W. Kui, *Acta. Metall. Mater.* **1993**, *43*, 1999.
[17] C. F. Lau, H. W. Kui, *Acta Metall. Mater.* **1994**, *42*, 3811.
[18] S. K. Mishra, S. Satpathy, *Physica B (Amsterdam, Neth.)* **1998**, *254*, 234.
[19] J. L. Maurice, *Philos. Mag. A* **1993**, *68*, 951.
[20] C. Wild, P. Koidl, W. Muller-Sebert, H. Walcher, R. Kohl, N. Herres, R. Locher, R. Samlenski, R. Brenn, *Diamond Relat. Mater.* **1993**, *2*, 158.
[21] Y. Matukura, *Jpn. J. Appl. Phys.* **1963**, *2*, 91.
[22] V. Dutta, P. Nath, K. L. Chopra, *Phys. Status Solidi* **1978**, *48*, 257.
[23] G. L. Pearson, W. T. Read Jr., F. J. Morin, *Phys. Rev.* **1954**, *93*, 666.
[24] A. G. Tweet, *Phys. Rev.* **1955**, *99*, 1245.
[25] D. J. Dumin, *Vac. Sci. Technol.* **1969**, *6*, 498.
[26] P. N. Grillot, S. A. Ringel, J. Michel, E. A. Fitzgerald, *J. Appl. Phys.* **1996**, *80*, 2823.
[27] L. P. Scheller, M. Weizman, N. H. Nickel, B. Yan, *Appl. Phys. Lett.* **2009**, *95*, 062101-1.